

Unified picture of the doping dependence of superconducting transition temperatures in alkali metal/ammonia intercalated FeSe

Daniel Guterding,^{1,*} Harald O. Jeschke,¹ P. J. Hirschfeld,² and Roser Valentí¹

¹*Institut für Theoretische Physik, Goethe-Universität Frankfurt,
Max-von-Laue-Straße 1, 60438 Frankfurt am Main, Germany*

²*Department of Physics, University of Florida, Gainesville, Florida 32611, U.S.A.*

In the recently synthesized $\text{Li}_x(\text{NH}_2)_y(\text{NH}_3)_z\text{Fe}_2\text{Se}_2$ family of iron chalcogenides a molecular spacer consisting of lithium ions, lithium amide and ammonia separates layers of FeSe. It has been shown that upon variation of the chemical composition of the spacer layer, superconducting transition temperatures can reach $T_c \sim 44$ K, but the relative importance of the layer separation and effective doping to the T_c enhancement is currently unclear. Using state of the art band structure unfolding techniques, we construct eight-orbital models from *ab-initio* density functional theory calculations for these materials. Within an RPA spin-fluctuation approach, we show that the electron doping enhances the superconducting pairing, which is of s_{\pm} -symmetry and explain the experimentally observed limit to T_c in the molecular spacer intercalated FeSe class of materials.

PACS numbers: 71.15.Mb, 71.18.+y, 71.20.-b, 74.20.Pq, 74.24.Ha, 74.70.Xa

After the discovery of iron based superconductors in 2008, transition temperatures were quickly improved to ~ 56 K by chemical substitution¹. Recently, the possible discovery of superconductivity with $T_c = 65$ K² and even $T_c \sim 100$ K³ in single-layer FeSe films grown by molecular beam epitaxy on SrTiO_3 showed that temperatures close to and above the boiling point of liquid nitrogen (77 K) might be achievable. These results have initiated an intensive debate regarding the origin of the high superconducting temperatures and the role played by electron doping via substrate, dimensionality and lattice strain.

While bulk FeSe has a T_c of only 8-10 K, it has been known for some time that it can be substantially enhanced, to 40 K or higher by alkali intercalation⁴. Materials with a single alkali $A = \text{K}, \text{Cs}, \text{Rb}$ between FeSe layers of nominal form $A_x\text{Fe}_{2-y}\text{Se}_2$ have been intensively studied, and shown to display a wide variety of unusual behaviors relative to the Fe pnictide superconducting materials⁵. These include likely phase separation into an insulating phase with block antiferromagnetism and ordered Fe vacancies, and a superconducting phase that is strongly alkali deficient and whose Fermi surface as measured by ARPES apparently contains no holelike Fermi surface pockets, in contrast to Fe-pnictides. Since the popular spin fluctuation scenario for s_{\pm} pairing relies on near nesting of hole and electron pockets, it has been speculated that a different mechanism for pairing might be present in these materials, and even within the spin fluctuation approach, different gap symmetries including d -wave pairing have been proposed⁶⁻⁹. The gap symmetry and structure is still controversial, however^{10,11}.

In addition to the unusual doping, speculation on the origin of the higher T_c has centered on the intriguing possibility that enhancing the FeSe layer spacing improves the two-dimensionality of the band structure and hence Fermi surface nesting^{12,13}. In an effort to investigate this latter effect, organic molecular complexes including alkalis were recently intercalated between the FeSe layers¹²⁻¹⁹, yielding transition temper-

atures up to 46 K. The most intensively studied materials incorporate molecules including ammonia, for example $\text{Li}_{0.56}(\text{NH}_2)_{0.53}(\text{NH}_3)_{1.19}\text{Fe}_2\text{Se}_2$ with $T_c = 39$ K¹⁴ and $\text{Li}_{0.6}(\text{NH}_2)_{0.2}(\text{NH}_3)_{0.8}\text{Fe}_2\text{Se}_2$ with $T_c = 44$ K¹⁵. The crystal structure of a stoichiometric version of these materials is shown in Fig. 1. Recently, Noji *et al.*¹³ compared data on a wide variety of FeSe intercalates and noted a strong correlation of T_c with interlayer spacing, corresponding to a nearly linear increase between 5 to 9 Å, followed by a rough independence of spacing with further increase between 9 to 12 Å.

In the present work we study the question of how exactly doping and interlayer distance influence T_c in molecular intercalates of FeSe, whether these effects are separable, and what gives rise to the apparent upper limit for T_c in this family of iron chalcogenides. Using a combination of first principles calculations of the electronic structure of several materials in this class, together with model calculations of spin fluctuation pairing based on these band structures, we argue that strength and wavevector of spin-fluctuations in lithium/ammonia intercalated FeSe can be controlled by tuning the $\text{Li}^+:\text{NH}_2^-$ ratio in the spacer layer. We show that the evolution of T_c with electron doping can be understood from the shape of the density of states close to the Fermi level. As long as hole pockets are present, we find that the superconducting pairing is of s_{\pm} character and identify a subleading $d_{x^2-y^2}$ instability. We believe that our interpretation is valid in a broad class of related materials.

We performed density functional theory calculations for $\text{Li}_{0.5}(\text{NH}_2)_y(\text{NH}_3)_z\text{Fe}_2\text{Se}_2$ at various ratios of NH_2^- to NH_3 content, starting from the experimentally determined structures $\text{Li}_{0.56}(\text{NH}_2)_{0.53}(\text{NH}_3)_{1.19}$ ¹⁴ and $\text{Li}_{0.6}(\text{NH}_2)_{0.2}(\text{NH}_3)_{0.8}$ ¹⁵, which include fractionally occupied atomic sites for lithium, hydrogen and nitrogen. In order to accommodate the experimental stoichiometry we construct a $2 \times 1 \times 1$ (4 Fe) supercell for the former, and a $2 \times 2 \times 1$ (8 Fe) supercell for the latter compound. We replace all fractionally occupied nitrogen positions by

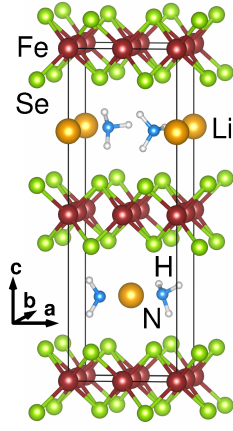


FIG. 1. (Color online) Idealized crystal structure of $\text{Li}_{0.5}(\text{NH}_3)\text{Fe}_2\text{Se}_2$. For a detailed discussion of experimental crystal structures see Ref. 14 and 15.

fully occupied positions. As hydrogen positions are not known precisely from experiment, we arrange the hydrogen atoms so that we obtain NH_3 groups with angles of about 108° as encountered in ammonia and further relax these positions within the local density approximation (LDA)²⁰ with the projector augmented wave (PAW) basis²¹ as implemented in GPAW²² until forces are below $2 \text{ meV}/\text{\AA}$. In the $2 \times 1 \times 1$ supercell we place the lithium atom in one half of the unit cell and leave the lithium position in the other half unoccupied. In the $2 \times 2 \times 1$ supercell we arrange the lithium atoms in a checkerboard pattern of occupied and vacant sites (Fig. 1).

Initially, we only consider charge neutral NH_3 ammonia groups in the spacer and no NH_2^- . In this way, we obtain idealized structures with formula units $\text{Li}_{0.5}(\text{NH}_3)\text{Fe}_2\text{Se}_2$ and $\text{Li}_{0.5}(\text{NH}_3)_2\text{Fe}_2\text{Se}_2$ where chalcogen height and unit cell parameters are chosen as in the experimental structures^{14,15}. Both structures belong to the space group P1 because of NH_3 situated in the spacer layer. Note that by setting up both structures with neutral NH_3 , we are able to disentangle possible effects of the structural differences from the effect of doping through the composition of the spacer layer.

The experimentally available samples^{14,15} contain both NH_3 and NH_2^- . The radical NH_2^- neutralizes the charge donated to the FeSe layer by Li^+ and reduces the doping level. In order to capture this compensation of charge in our simulations, we use the virtual crystal approximation (VCA)²³ starting from supercells $\text{Li}_{0.5}(\text{NH}_3)\text{Fe}_2\text{Se}_2$ and $\text{Li}_{0.5}(\text{NH}_3)_2\text{Fe}_2\text{Se}_2$, which correspond to the maximally electron doped compounds. The use of VCA has the advantage that doping is treated in a continuous and rather isotropic, but not rigid band fashion. We checked these calculations by removing hydrogen atoms explicitly instead of doing VCA and found the differences to be negligible.

The analysis of the band structure of these supercells is done within an all electron full potential local orbital

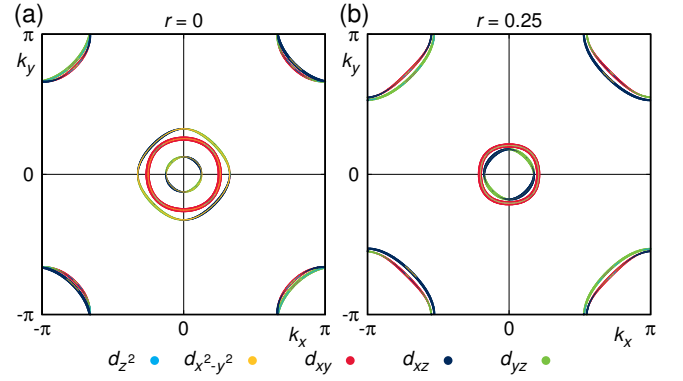


FIG. 2. (Color online) Fermi surface in the 16 band tight binding model for $r = 0.0$ (a) and $r = 0.25$ (b) in the 2-Fe Brillouin zone at $k_z = 0$. The colors indicate the weights of the Fe 3d states.

(FPLO)²⁴ basis and we use LDA as exchange-correlation functional²⁰. We then use projective Wannier functions as implemented in FPLO²⁵ to downfold the band structure. In our tight binding models, we keep the Fe 3d and Se 4p states. In order to obtain band structure and Fermi surface of the supercells in the conventional two iron unit cell, we use our recently developed technique²⁶ to translationally unfold the 32 and 64 band supercell models to a 16 band model of the 2 Fe equivalent Brillouin zone. For calculations of susceptibility and superconducting pairing, we use subsequent glide reflection unfolding²⁶ of the bands to obtain the 8 band model of the 1 Fe equivalent Brillouin zone.

First we investigated the properties of the maximally electron doped compounds in our study, $\text{Li}_{0.5}(\text{NH}_3)\text{Fe}_2\text{Se}_2$ (ammonia poor) and $\text{Li}_{0.5}(\text{NH}_3)_2\text{Fe}_2\text{Se}_2$ (ammonia rich). Both feature at the Fermi level (not shown) two large electron pockets in the corners of the 2 Fe Brillouin zone and two small hole pockets around Γ . This confirms that the lithium atoms donate electrons to the FeSe layer. Both systems have the same electron doping but different interlayer spacing. This is observed in the k_z -dispersion of the Fermi surface, where the smaller interlayer distance of the ammonia poor compound leads to a slightly increased corrugation of the cylinders.

In the experimentally realized compounds $\text{Li}_{0.56}(\text{NH}_2)_{0.53}(\text{NH}_3)_{1.19}$ and $\text{Li}_{0.6}(\text{NH}_2)_{0.2}(\text{NH}_3)_{0.8}$ the spacer layer nominally donates a charge of 0.015 and 0.2 electrons per iron atom respectively. These doping levels are lower than in our model materials $\text{Li}_{0.5}(\text{NH}_3)\text{Fe}_2\text{Se}_2$ and $\text{Li}_{0.5}(\text{NH}_3)_2\text{Fe}_2\text{Se}_2$. To investigate the doping dependence of the electronic structure at a given interlayer spacing, we consider $\text{Li}_{0.5}(\text{NH}_3)\text{Fe}_2\text{Se}_2$ and hole dope it by means of the virtual crystal approximation as explained above. To simplify the notation, we label compounds from now on not by their full chemical formula, but by an index $r = \{0.0, \dots, 0.25\}$, which refers to the chemical formula

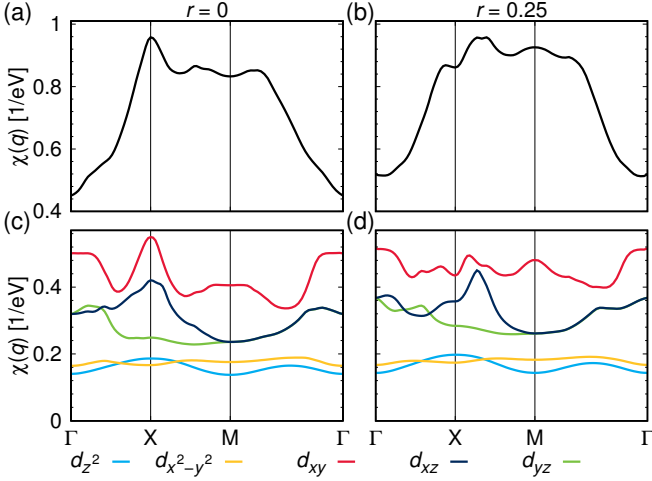


FIG. 3. (Color online) Summed static susceptibility (upper panel) and its diagonal components χ_{aa}^{aa} (lower panel) in the 8 band tight binding model for $r = 0.0$ (a,c) and $r = 0.25$ (b,d) in the 1-Fe Brillouin zone. The colors identify the Fe 3d states.

$\text{Li}_{0.5}(\text{NH}_2)_{0.5-2r}(\text{NH}_3)_{0.5+2r}\text{Fe}_2\text{Se}_2$. $r = 0.25$ refers to the compound $\text{Li}_{0.5}(\text{NH}_3)\text{Fe}_2\text{Se}_2$ with maximal electron doping, where lithium nominally transfers a quarter of an electron to each iron atom. Increasing the NH_2^- content immediately brings up a third hole pocket to the Fermi level, which is three-dimensional at intermediate doping and becomes two-dimensional once the charge introduced by lithium is fully compensated by NH_2^- groups. $r = 0$ denotes the compound where the charge introduced by lithium is nominally compensated by NH_2^- and no electrons are donated to the FeSe layer. The Fermi surfaces of the end members ($r = 0.0$ and $r = 0.25$) are shown in Fig. 2. The band structure on high-symmetry paths is included in the Supplemental Material²³.

Upon further analysis of the tight-binding parameters we find that the hole pockets do not only shrink because the electron doping raises the Fermi level, but also because the nearest neighbor hopping in the Fe 3d_{xy} orbital decreases steeply as a function of electron doping. This near cancellation of direct and indirect hopping paths has been discussed in the literature for other iron based superconductors²⁷⁻²⁹. In the materials investigated here, we find that the degree of localization in the Fe 3d_{xy} orbital can be tuned with relatively low electron doping. Further information are given in the Supplemental Material²³.

Next, we investigate the doping dependence of spin fluctuations. The non-interacting static susceptibility on the high-symmetry path calculated in the 1-Fe Brillouin zone for $r = 0.0$ and $r = 0.25$ is shown in Fig. 3. The susceptibility χ_{st}^{pq} is a four-tensor in orbital indices. The observable static susceptibility is defined as the sum over all components χ_{aa}^{bb} . In the undoped compound ($r = 0.0$) the structure of the static susceptibility resembles strongly

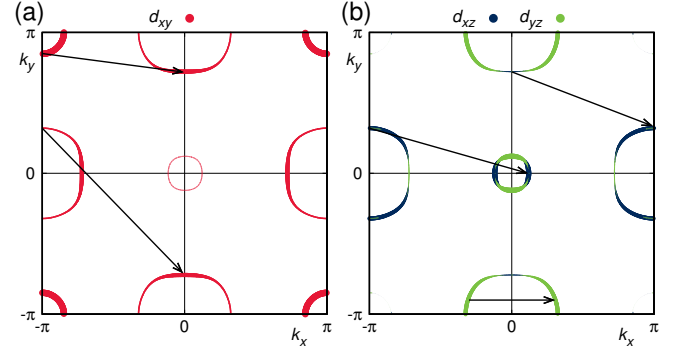


FIG. 4. (Color online) Fermi surface in the 8 band tight binding model for $r = 0.25$ in the 1-Fe Brillouin zone at $k_z = 0$. Shown are the orbital characters for the d_{xy} (a) and the d_{xz/yz} (b) orbitals. The arrows represent dominant interaction vectors identified from peaks in the susceptibility.

what is found for materials like LaFeAsO or BaFe₂As₂. The electron doping notably shifts the maximum from $X = (\pi, 0)$ towards $M = (\pi, \pi)$ and the former valley at M transforms into a peak. The absence of a $(\pi, 0)$ peak in electron doped compounds suggests why no orthorhombic phase or stripe-like magnetism have been found in FeSe intercalates so far³⁰.

The shifts of the dominant vectors of spin fluctuations can be understood from nesting properties and orbital character on the Fermi surface in the 1-Fe Brillouin zone. The undoped compound ($r = 0.0$) is dominated by $(\pi, 0)$ nesting of electron and hole pockets, whereas the electron doped compound ($r = 0.25$) (see Fig. 4) features scattering between electron and hole pockets with altered wave vector competing with scattering between electron pockets. The dominant contributions to the static susceptibility originate from the d_{xy} and d_{xz/yz} orbitals.

To explore how the superconducting state might depend on interlayer spacing and doping, we use the 3D version of random phase approximation (RPA) spin fluctuation theory³¹ with Hamiltonian $H = H_0 + H_{int}$. Here H_0 is the tight-binding Hamiltonian derived from the DFT calculations using the projective Wannier function formalism described above, and H_{int} is the Hubbard-Hund interaction, including the onsite intra (inter) orbital Coulomb interaction U (U'), the Hund's rule coupling J and the pair hopping energy J' . We keep the selenium states in the entire calculation, but consider interactions only between Fe 3d states. We assume spin rotation-invariant interaction parameters $U = 1.35$ eV, $U' = U/2$, $J = J' = U/4$. The effective interaction in the singlet pairing channel is then constructed via the multiorbital RPA procedure. Both the original Hamiltonian and effective interaction are discussed, e.g. in Ref. 32.

For all values of electron doping (structures $r = 0.0$ to $r = 0.25$) and interlayer spacing (structures $\text{Li}_{0.5}(\text{NH}_3)\text{Fe}_2\text{Se}_2$ and $\text{Li}_{0.5}(\text{NH}_3)_2\text{Fe}_2\text{Se}_2$) considered we find the leading instability to be of nodeless s_{\pm} character,

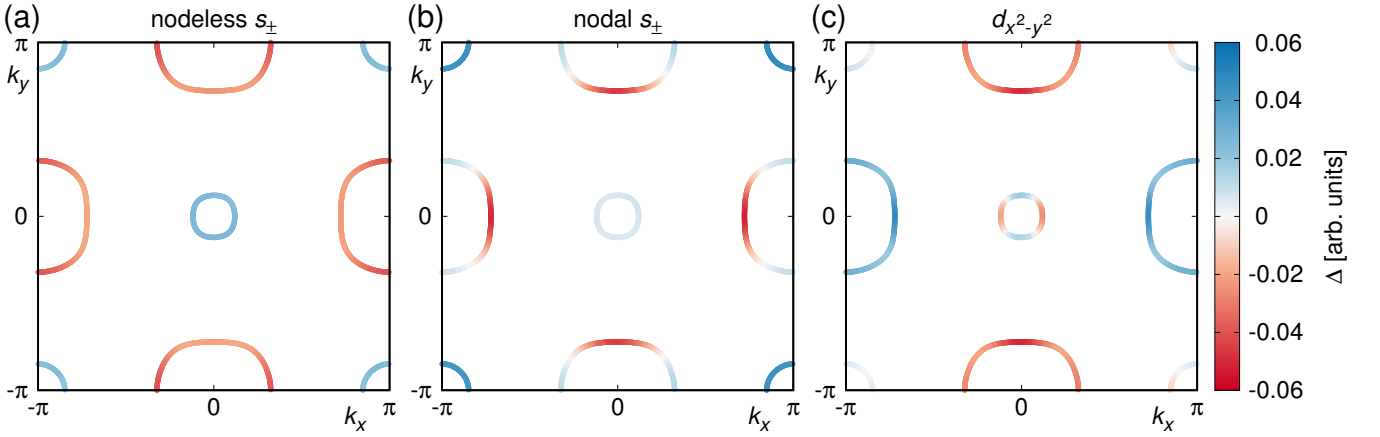


FIG. 5. (Color online) Solutions of the linearized gap equation on the Fermi surface within the 8 band tight binding model for $r = 0.25$ in the 1-Fe Brillouin zone at $k_z = 0$. The relevant instabilities are nodeless s_{\pm} (a), nodal s_{\pm} (b) and $d_{x^2-y^2}$ (c). We assume spin rotation-invariant interaction parameters $U = 1.35$ eV, $U' = U/2$, $J = J' = U/4$.

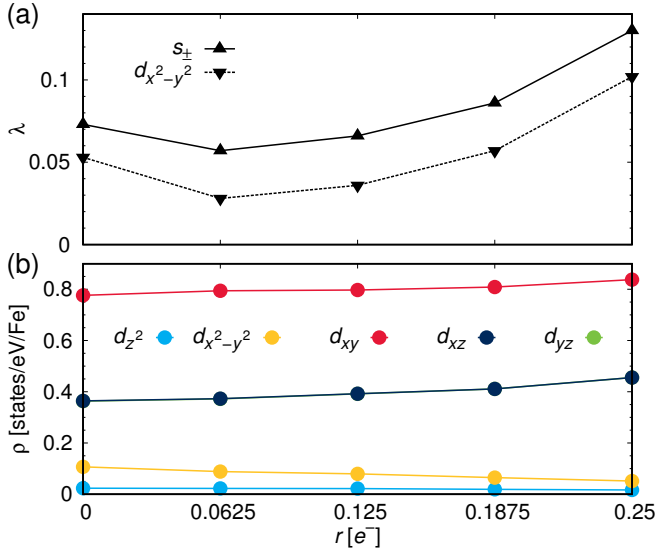


FIG. 6. (Color online) Trend of the eigenvalues of s_{\pm} and $d_{x^2-y^2}$ solutions (a) and orbital resolved Fe 3d density of states at the Fermi level (b) with doping.

while subleading solutions are of nodal s_{\pm} and $d_{x^2-y^2}$ type (see Fig. 5 for structure $r = 0.25$). These are the leading states expected in the case of a nearly 2D system with both hole and electron pockets. Repulsive electron-hole $d_{xz/yz}$ and d_{xy} interactions favor nodeless s_{\pm} pairing, while interelectron pocket interactions, orbital weight variations around the Fermi surface, and intraband Coulomb interactions are known to frustrate the s_{\pm} interaction and drive nodal behavior and eventually d -wave interactions when hole pockets disappear^{8,33}.

We observe that the source of the moderate quantitative enhancement of T_c with electron doping lies in an increased density of states at the Fermi level. For both the d_{xy} and the $d_{xz/yz}$ orbitals the slope of density

of states near the Fermi level is positive (Fig. 6 (b)) so that electron doping leads to an enhanced susceptibility and superconducting pairing strength as the doping approaches the edge of the hole bands, which appears as a sharp drop of the d_{xy} DOS²³. The small initial decrease of the pairing eigenvalue at low electron doping (Fig. 6 (a)) is a consequence of the degraded nesting.

Alternatively, when we keep the electron doping levels fixed to the same value and analyze only the inter-layer spacing effect (structures $\text{Li}_{0.5}(\text{NH}_3)\text{Fe}_2\text{Se}_2$ with $c = 8.1$ Å and $\text{Li}_{0.5}(\text{NH}_3)_2\text{Fe}_2\text{Se}_2$ with $c = 10.3$ Å), we find that the Fermi surface turns completely two-dimensional for a c -axis length between 8.1 Å and 10.3 Å, where T_c saturates in experiment. Analyzing the susceptibility and superconducting pairing for both structures, we find no qualitative differences. Quantitatively, the perfectly two-dimensional Fermi surface of the ammonia rich compound leads to an increased susceptibility and larger pairing eigenvalue than in the ammonia poor compound. The increased pairing eigenvalue would correspond to an enhanced T_c .

Our calculations show that both increasing electron doping and lattice spacing contribute to enhancing T_c . However, experimentally it is found that the ammonia poor compound (larger electron doping) with smaller c -axis shows a higher T_c ($\text{Li}_{0.6}(\text{NH}_2)_{0.2}(\text{NH}_3)_{0.8}\text{Fe}_2\text{Se}_2$, $T_c = 44$ K) than the ammonia rich compound (smaller electron doping) with larger c -axis ($\text{Li}_{0.56}(\text{NH}_2)_{0.53}(\text{NH}_3)_{1.19}\text{Fe}_2\text{Se}_2$, $T_c = 39$ K). Therefore, the variations in lattice parameters observed experimentally cannot be the source of the enhancement of T_c . Within our picture, this leaves only the electron doping level as the controlling parameter. Hence we conclude that T_c is mainly controlled by the electron doping level when the Fermi surface is mostly two-dimensional. Therefore it is unlikely that T_c can be enhanced further by intercalation of larger molecules.

Summarizing, we investigated the

$\text{Li}_x(\text{NH}_2)_y(\text{NH}_3)_z\text{Fe}_2\text{Se}_2$ family of FeSe intercalates and found that the FeSe layer is moderately electron doped. The electron doping moves the Fermi level towards the edge of the hole-bands, which gives rise to increased superconducting transition temperatures due to an increase in the density of states at the Fermi level. We also showed that recently achieved inter-layer distances in FeSe intercalates already produce a two-dimensional Fermi surface, which is optimal for T_c . Further experimental work should therefore concentrate on the charge doping through the spacer layer.

We would like to thank Stephen J. Blundell and Simon J. Clarke for pointing this interesting problem to us and Milan Tomić and Andreas Kreisel for useful discussions. We thank the Deutsche Forschungsgemeinschaft for financial support through Grant No. SPP 1458. This research was supported in part by the National Science Foundation under Grant No. PHY11-25915. PJH and RV thank the Kavli Institute for Theoretical Physics at the University of California, Santa Barbara for the kind hospitality. PJH acknowledges support by the Department of Energy under Grant No. DE-FG02-05ER46236.

-
- * guterding@itp.uni-frankfurt.de
- ¹ G. Wu, Y. L. Xie, H. Chen, M. Zhong, R. H. Liu, B. C. Shi, Q. J. Li, X. F. Wang, T. Wu, Y. J. Yan, J. J. Ying, and X. H. Chen, *J. Phys.: Condens. Matter* **21**, 142203 (2009).
 - ² S. Tan, Y. Zhang, M. Xia, Z. Ye, F. Chen, X. Xie, R. Peng, D. Xu, Q. Fan, H. Xu, J. Jiang, T. Zhang, X. Lai, T. Xiang, J. Hu, B. Xie, and D. Feng, *Nat. Mater.* **12**, 634 (2013).
 - ³ J.-F. Ge, Z.-L. Liu, C. Liu, C.-L. Gao, D. Qian, Q.-K. Xue, Y. Liu, and J.-F. Jia, *Nat. Mater.*, 10.1038/nmat4153.
 - ⁴ J. Guo, S. Jin, G. Wang, S. Wang, K. Zhu, T. Zhou, M. He, and X. Chen, *Phys. Rev. B* **82**, 180520 (2010).
 - ⁵ E. Dagotto, *Rev. Mod. Phys.* **85**, 849 (2013).
 - ⁶ F. Wang, F. Yang, M. Gao, Z.-Y. Lu, T. Xiang, and D.-H. Lee, *Europhys. Lett.* **93**, 57003 (2011).
 - ⁷ T. A. Maier, S. Graser, P. J. Hirschfeld, and D. J. Scalapino, *Phys. Rev. B* **83**, 100515 (2011).
 - ⁸ S. Maiti, M. M. Korshunov, T. A. Maier, P. J. Hirschfeld, and A. V. Chubukov, *Phys. Rev. Lett.* **107**, 147002 (2011).
 - ⁹ A. Kreisel, Y. Wang, T. A. Maier, P. J. Hirschfeld, and D. J. Scalapino, *Phys. Rev. B* **88**, 094522 (2013).
 - ¹⁰ M. Xu, Q. Q. Ge, R. Peng, Z. R. Ye, J. Jiang, F. Chen, X. P. Shen, B. P. Xie, Y. Zhang, A. F. Wang, X. F. Wang, X. H. Chen, and D. L. Feng, *Phys. Rev. B* **85**, 220504 (2012).
 - ¹¹ I. I. Mazin, *Phys. Rev. B* **84**, 024529 (2011).
 - ¹² E.-W. Scheidt, V. R. Hathwar, D. Schmitz, A. Dunbar, W. Scherer, F. Mayr, V. Tsurkan, J. Deisenhofer, and A. Loidl, *Eur. Phys. J. B* **85**, 279 (2012).
 - ¹³ T. Noji, T. Hatakeda, S. Hosono, T. Kawamata, M. Kato, and Y. Koike, *Physica C* **504**, 8 (2014).
 - ¹⁴ S. J. Sedlmaier, S. J. Cassidy, R. G. Morris, M. Drakopoulos, C. Reinhard, S. J. Moorhouse, D. O'Hare, P. Manuel, D. Khalyavin, and S. J. Clarke, *J. Am. Chem. Soc.* **136**, 630 (2014).
 - ¹⁵ M. Burrard-Lucas, D. G. Free, S. J. Sedlmaier, J. D. Wright, S. J. Cassidy, Y. Hara, A. J. Corkett, T. Lancaster, P. J. Baker, S. J. Blundell, and S. J. Clarke, *Nat. Mater.* **12**, 15 (2013).
 - ¹⁶ H. Sun, D. N. Woodruff, S. J. Cassidy, G. M. Allcroft, S. J. Sedlmaier, A. L. Thompson, P. A. Bingham, S. D. Forder, S. Cartenet, N. Mary, S. Ramos, F. R. Foronda, B. J. Williams, X. Li, S. J. Blundell, and S. J. Clarke, *arXiv:1408.4350* (unpublished).
 - ¹⁷ T. P. Ying, X. L. Chen, G. Wang, S. F. Jin, T. T. Zhou, X. F. Lai, H. Zhang, and W. Y. Wang, *Sci. Rep.* **2**, 426 (2012).
 - ¹⁸ A. Krzton-Maziopa, E. V. Pomjakushina, V. Yu. Pomjakushin, F. von Rohr, A. Schilling, and K. Conder, *J. Phys.: Condens. Matter* **24**, 382202 (2012).
 - ¹⁹ J. Guo, H. Lei, F. Hayashi, and H. Hosono, *Nat. Commun.* **5**, 4756 (2014).
 - ²⁰ J. P. Perdew and Y. Wang, *Phys. Rev. B* **45**, 13244 (1992).
 - ²¹ P. E. Blöchl, *Phys. Rev. B* **50**, 17953 (1994).
 - ²² J. Enkovaara, C. Rostgaard, J. J. Mortensen *et al.*, *J. Phys.: Condens. Matter* **22**, 253202 (2010); <https://wiki.fysik.dtu.dk/gpaw>
 - ²³ See Supplemental Material at [URL will be inserted by publisher], which includes further information on the *ab-initio* calculations, the model construction and the susceptibility and pairing calculations. Furthermore, it connects kinetic frustration with the increased density of states.
 - ²⁴ K. Koepnick and H. Eschrig, *Phys. Rev. B* **59**, 1743 (1999); <http://www.FPLO.de>
 - ²⁵ H. Eschrig and K. Koepnick, *Phys. Rev. B* **80**, 104503 (2009).
 - ²⁶ M. Tomić, H. O. Jeschke, and R. Valentí, *Phys. Rev. B* **90**, 195121 (2014).
 - ²⁷ Z. P. Yin, K. Haule, and G. Kotliar, *Nat. Mater.* **10**, 932 (2011).
 - ²⁸ K. Suzuki, H. Usui, S. Iimura, Y. Sato, S. Matsuishi, H. Hosono, and K. Kuroki, *Phys. Rev. Lett.* **113**, 027002 (2014).
 - ²⁹ O. K. Andersen and L. Boeri, *Ann. Phys. (Berlin)* **523**, 8 (2011).
 - ³⁰ A. E. Taylor, S. J. Sedlmaier, S. J. Cassidy, E. A. Goremychkin, R. A. Ewings, T. G. Perring, S. J. Clarke, and A. T. Boothroyd, *Phys. Rev. B* **87**, 220508 (2013).
 - ³¹ S. Graser, T. A. Maier, P. J. Hirschfeld, and D. J. Scalapino, *New J. Phys.* **11**, 025016 (2009).
 - ³² P. J. Hirschfeld, M. M. Korshunov, and I. I. Mazin, *Rep. Prog. Phys.* **74**, 124508 (2011).
 - ³³ T. A. Maier, S. Graser, D. J. Scalapino, and P. J. Hirschfeld, *Phys. Rev. B* **79**, 224510 (2009).

Unified picture of the doping dependence of superconducting transition temperatures in alkali metal/ammonia intercalated FeSe: Supplemental Information

Daniel Guterding,^{1,*} Harald O. Jeschke,¹ P. J. Hirschfeld,² and Roser Valentí¹

¹*Institut für Theoretische Physik, Goethe-Universität Frankfurt,
Max-von-Laue-Straße 1, 60438 Frankfurt am Main, Germany*

²*Department of Physics, University of Florida, Gainesville, Florida 32611, U.S.A.*

I. DETAILS OF THE AB-INITIO CALCULATION

For the relaxation of crystal structures we used $6 \times 6 \times 6$ k-point grids within the GPAW code. The structure optimization process was controlled by the Broyden-Fletcher-Goldfarb-Shanno (BFGS) algorithm implemented in the Python atomic simulation environment (ASE)¹. We checked the remaining forces in the full potential local orbital code FPLO with a $12 \times 12 \times 12$ k-point mesh and found the atomic positions to be sufficiently converged. All further calculations using FPLO were carried out on $12 \times 12 \times 12$ k-point meshes.

We investigated the doping dependence of the electronic structure by means of the virtual crystal approximation (VCA). The VCA can be used to interpolate continuously between the properties of an atom with nuclear charge Z and its neighbors in the periodic table of elements with nuclear charges $Z - 1$ or $Z + 1$. In the study presented here, we fractionally replaced nitrogen ($Z = 7$) by carbon ($Z = 6$). Because of the different valence of nitrogen and carbon this procedure interpolates between charge neutral ammonia (NH_3) and a methyl radical (CH_3^\cdot). As ammonia (NH_3) and methane (CH_4) are structurally similar, VCA should provide a sufficient description of the spacer layer.

II. DETAILS OF THE MODEL CONSTRUCTION

We obtained the low energy Hamiltonian for each doping level from *ab-initio* calculations and subsequent Wannier downfolding using the FPLO Wannier module. We keep all Fe $3d$ and Se $4p$ states in our models. For the 8 Fe supercell this process yields a 64 band tight binding model, which we then treat with the unfolding methods described in the main text. The energy window we used for the fit spans approximately from -6 eV to $+2$ eV.

In FPLO a direct unfolding of the DFT band weights is implemented². We used it to check agreement between unfolded DFT band structure and unfolded model band structure in the 2 Fe picture to exclude uncertainties from the Wannierization procedure. The only case where we found small quantitative deviations close to the Fermi level is the $\text{Li}_{0.5}(\text{NH}_{2.5})\text{Fe}_2\text{Se}_2$ ($r = 0$) compound, where a nitrogen band at -1.5 eV prevents a perfect fit using Fe $3d$ and Se $4p$ states only.

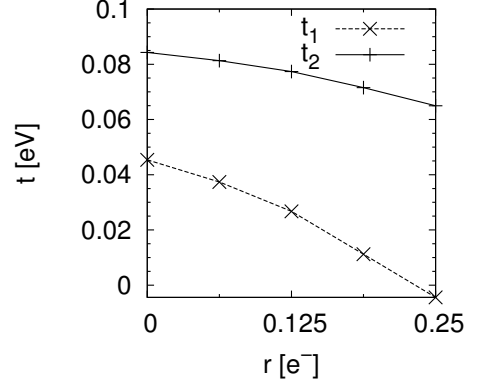


FIG. 1. Nearest and next-nearest neighbor hopping (t_1 and t_2 respectively) in the Fe $3d_{xy}$ orbital within a 5 band iron only picture.

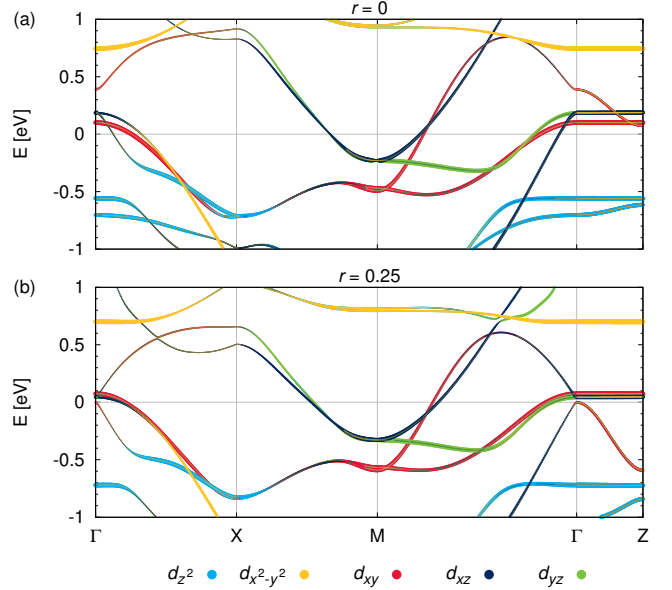


FIG. 2. Band structure in the 16 band tight binding model for $r = 0.0$ (a) and $r = 0.25$ (b) in the 2-Fe Brillouin zone. The colors indicate the weights of Fe $3d$ states.

III. DETAILS OF THE SUSCEPTIBILITY AND PAIRING CALCULATION

The static susceptibility is calculated on a $30 \times 30 \times 10$ k-point mesh at an inverse temperature of $\beta = 40$ eV⁻¹. To calculate the pairing interaction, the susceptibility is

needed at k -vectors that do in general not lie on a grid. Those susceptibility values are obtained using trilinear interpolation of the gridded data.

The gap equation is solved using ~ 1000 points on the three-dimensional Fermi surface. Consequently the solution of the gap equation is available only on those points scattered in three-dimensional space. In order to obtain a graphical representation of the gap function on two-dimensional cuts through the Brillouin zone, we used multiscale radial basis function interpolation as implemented in ALGLIB (<http://www.alglib.net>).

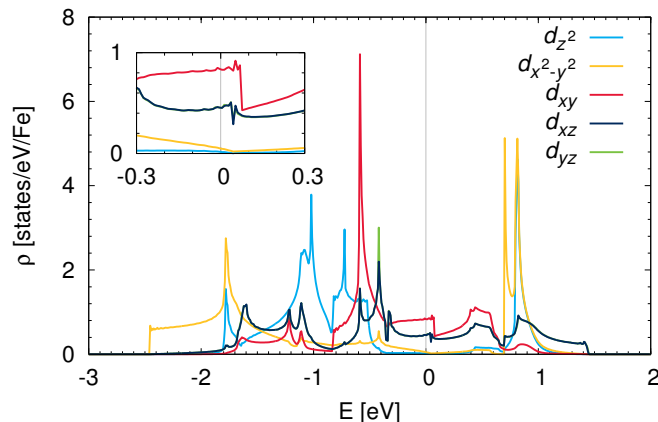


FIG. 3. Orbital resolved Fe $3d$ density of states of the 8 band tight binding model for $r = 0.25$.

IV. ROLE OF KINETIC FRUSTRATION

An alternative way of understanding the variation in pairing strength with electron doping is provided through

the analysis of the tight binding parameters. As mentioned in the main text, we observe a steep decrease of the nearest neighbor hopping with electron doping. To allow easy interpretation of the hopping elements, we constructed 5 band Fe only models by downfolding also the Se $4p$ states. We used an energy window ranging from -3 eV to $+2$ eV.

As shown in Fig. 1, the nearest neighbor hopping t_1 is affected much stronger by the electron doping than the next-nearest neighbor hopping t_2 . This behavior has been explained in the literature by the cancellation of direct and indirect hopping paths via the chalcogen atoms³. Recently, similar arguments were used to explain the doping dependence of superconductivity in $\text{LaFeAsO}_{1-x}\text{H}_x$ and related materials⁴. In the intercalates we investigated, we find rather small Fe $3d_{xy}$ hoppings because of the large Se height of 1.476 Å, which reduces indirect hoppings via the Se atoms.

The band structure effects of changing individual hopping parameters have been worked out in great detail in Ref. 5. In the materials investigated here, the change in t_1 serves to shift the hole bands down (Fig. 2), which gives rise to the increased density of states at the Fermi level.

V. DENSITY OF STATES

In Fig. 3 we plot the orbital resolved density of states for the 8 band model at $r = 0.25$. The positive slope close to the Fermi level and the edge of the hole bands at $+0.1$ eV are clearly visible.

* guterding@itp.uni-frankfurt.de

¹ S. R. Bahn and K. W. Jacobsen, Comput. Sci. Eng. **4**, 56 (2002); <https://wiki.fysik.dtu.dk/ase>

² W. Ku, T. Berlijn, and C.-C. Lee, Phys. Rev. Lett. **104**, 216401 (2010).

³ Z. P. Yin, K. Haule, and G. Kotliar, Nat. Mater. **10**, 932 (2011).

⁴ K. Suzuki, H. Usui, S. Iimura, Y. Sato, S. Matsuishi, H. Hosono, and K. Kuroki, Phys. Rev. Lett. **113**, 027002 (2014).

⁵ O. K. Andersen and L. Boeri, Ann. Phys. (Berlin) **523**, 8 (2011).